A Finite Element Model of a Microwave Catheter for Cardiac Ablation

Zouheir Kaouk, Ahmed Khebir, and Pierre Savard

Abstract—**To investigate the delivery of microwave energy by a catheter located inside the heart for the purpose of ablating small abnormal regions producing cardiac arrhythmias, a numerical model was developed. This model is based on the finite element method and can solve both the electromagnetic field and the temperature distribution resulting from the radiated power for axisymmetrical geometries. The antenna, which is fed by a coaxial cable with a 2.4 mm diameter, is constituted by a monopole which is terminated by a metallic cylindrical cap. The heart model can be either homogeneous or constituted of coaxial cylindrical shells with different electrical and thermal conductivities representing the intracavitary blood masses, the heart, and the torso. Experimental measurements obtained in an homogeneous tissue equivalent medium, such as the reflection coefficient of the antenna at different frequencies and for different monopole lengths, the radial and axial steady-state temperature profiles, and the time course of the temperature rise, were all in close agreement with the values computed with the model. Accurate modeling is a useful prerequisite for the design of antennas, and these results confirm the validity of the catheter-heart model for the investigation and the development of microwave catheters.**

I. Introduction

RADIO-FREQUENCY (RF) catheter ablation has been demonstrated to be highly successful for the treatment of supraventricular arrhythmias [1]. However, the lower success rates and clinical utilization [2] of RF catheter ablation for the treatment of ventricular tachycardias, which can originate deep within the myocardium [3], suggest the need for an alternative energy source that can ablate a greater volume of arrhythmogenic tissue. In contrast to RF energy which produces heat by conduction currents, microwave energy is delivered by a propagating electromagnetic wave with both conduction and displacement currents that offers the potential for greater lesion depths. Whayne *et al.* [4] investigated monopole antennas operating at 915 and 2450 MHz for microwave ablation of canine myocardium *in vitro*, and found that microwave lesion depths were indeed larger than those produced by RF energy. Rosenbaum *et al.* [5] also investigated helical and whip antennas with *in vivo* and phantom models in order to optimize the operating frequency and antenna design.

For cancer thermotherapy, numerical models have been developed [6]–[8] but none of them can be applied directly to cardiac catheter ablation. Specifically, the size of the antenna, the desired temperature levels, the radiation patterns, and the absence of large blood masses are quite different from those needed for modeling cardiac ablation. Recently, we have developed an electrothermal catheter-heart model to better understand RF and microwave energy delivery in the heart [9]. We found that the temperature distributions produced by microwave energy have a larger extent than those produced by RF energy delivered by the same catheter. In order to use this model for the development of new catheters with optimized antenna design, it is important to demonstrate its validity. In this paper, the numerical results obtained with the model are compared to experimental results obtained with a tissue equivalent medium as well as to recently published results [10].

Manuscript received November 6, 1995; revised April 1, 1996. This work was supported in part by the Natural Sciences and Engineering Research Council of Canada, and Fonds pour la Formation de Chercheurs et l'Aide à la Recherche du Québec.

The authors are with the Institute of Biomedical Engineering, Ecole Polytechnique and Université de Montréal, Montréal, PQ, Canada.

Publisher Item Identifier S 0018-9480(96)07019-6.

II. Description of the Model

The description of the numerical model with its different parameters was presented in a previous paper [9]. Briefly, the axisymmetrical model shown in Fig. 1 consists of three coaxial cylindrical shells which represent the intraventricular blood masses, the myocardium, and the torso. The catheter consists of a 50 Ω coaxial cable feeding an insulated loaded monopole antenna which was designed to provide enhanced tip heating. The antenna penetrates slightly into the myocardium (1 mm). The catheter radius is 1.2 mm. A thin dielectric sheath covers the outer conductor of the coaxial cable feedline.

For the finite element computations, using the vector Helmholtz equation along with the Galerkin method [11], the following weak form is obtained:

$$\int_V \nabla \times \boldsymbol{E} \cdot \nabla \times \boldsymbol{W_m}\, dV - \int_V k^2 \boldsymbol{E} \cdot \boldsymbol{W_m}\, dV + \int_S \boldsymbol{n} \times \nabla \times \boldsymbol{E} \cdot \boldsymbol{W_m}\, dS = 0 \quad (1)$$

where $\boldsymbol{W_m}$ are the vector weighting functions, $\boldsymbol{n}$ is the unit vector normal to the surface element dS, k is the complex wavenumber, V is the volume of the model, and S is the outer boundary. The variational equation (1) was discretized using the finite element method. Since the nodal approach is known to treat poorly the spurious and nonphysical modes, a hybrid edge element technique was used: for axisymmetrical geometries in the ϕ plane, the azimuthal direction is purely normal to the plane and a nodal representation was thus used for the azimuthal component, while an edge element representation was used for the transverse component [12]. The discontinuity of the coaxial cable at the radiating section

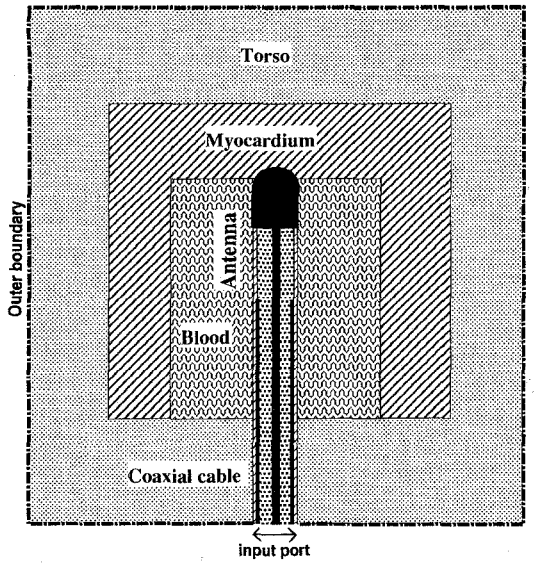

(a)

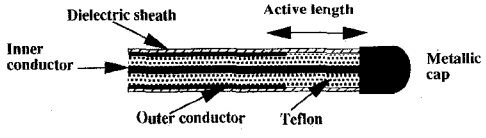

(b)

Fig. 1. (a) Schema of the axisymmetrical model. A coaxial cable feeds an insulated monopole located in a cylindrical cardiac chamber filled with blood and surrounded by a myocardial shell and a torso shell. (b) The antenna consists of an insulated monopole terminated by a metallic cap.

generates higher order modes inside the cable that do not propagate since the antenna dimensions are very small with respect to the wavelength at 2450 MHz. Furthermore, the input port shown in Fig. 1 is located far enough from the antenna junction to ensure that the evanescent modes are damped out. In this way, a first-order boundary condition is applied at the input port as follows [13]:

$$\frac{\partial \boldsymbol{E_t}(\boldsymbol{r})}{\partial z} = j\beta(\boldsymbol{E_t}(\boldsymbol{r}) - 2\boldsymbol{E^{inc}}) \tag{2}$$

where β is the propagation constant. A first-order radiation condition is applied to the remaining outer boundary [13]. The specific absorption rate (SAR) inside each medium was thus computed by solving Maxwell's equations using the vector-based finite element method to directly compute the electrical field assuming that the coaxial cable is excited by a single TEM mode. The temperature distribution T was finally calculated by solving the bio-heat equation using a node based finite element method since temperature is a scalar

$$\rho c_p \frac{\partial T}{\partial t} = \nabla \cdot (k \nabla T) + \frac{\sigma \boldsymbol{E}^2}{2} + Q_m + Q_p \tag{3}$$

where ρ is the medium density, and c_p is the specific heat; the first term on the right represents the thermal conduction, and k is the thermal conductivity; the second term on the right represents the dissipated power density, and σ is the electrical conductivity; Q_m and Q_p represent the metabolic heat sources and the heat loss due to the coronary blood flow,

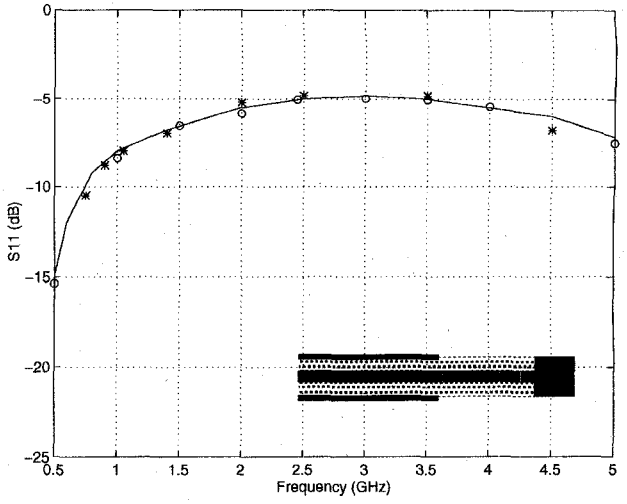

Fig. 2. Magnitude of the reflection coefficient S11 as a function of frequency: the continuous curve is a simulation result reported in [10]; the asterisks (*) are experimental values reported in [10]; and the o represents our simulated values. The same antenna geometry was used for the three approaches: a monopole terminated by a cylinder.

respectively. The last two terms were neglected because of the high energy levels and the coagulation within the microvessel encountered during catheter ablation (see Discussion). At the interface between the myocardium and the intraventricular blood masses, the following boundary condition was applied

$$k\frac{\partial T}{\partial n} = h_b(T - 37^\circ) \tag{4}$$

where the convection coefficient h_b was set at 1000 W/m^2°C by assuming that blood is flowing with a steady laminar flow at a constant temperature of 37°C [14]. Modeling the blood flow inside the heart chambers is a very difficult task due to the nonlinearity of the phenomena and due to the time and space dependence of blood velocity. So, as a first-order approximation, we assumed (as did others [15]) a laminar blood flow over the endocardium. For radio-frequency ablation, we have investigated the effect of varying the convection coefficient h_b (depends on blood velocity) and we have found no significant difference in heating depth when h_b is greater than 100 W/m^2°C. At the interface between the model and the air, a boundary condition similar to (4) was applied by assuming a slow laminar air flow at room temperature around the cylinder (h_a = 20 W/m^2°C).

III. Comparison to Published Results

Since the microwave ablation process consists of two coupled electrical and thermal phenomena, we validated the solutions to both of these problems. For the electrical aspect of the model, we computed the reflection coefficient S11 at the input port of the coaxial line by simulating the same geometry used by Labonté *et al.* [10] (i.e., a loaded monopole immersed in a 0.9% saline solution), who reported both experimental results and simulation results obtained with a node-based approach to find the magnetic field $\boldsymbol{H}$ and then derive the electric field $\boldsymbol{E}$. Fig. 2 shows both the calculated and the reported S11 as function of frequency. A good agreement

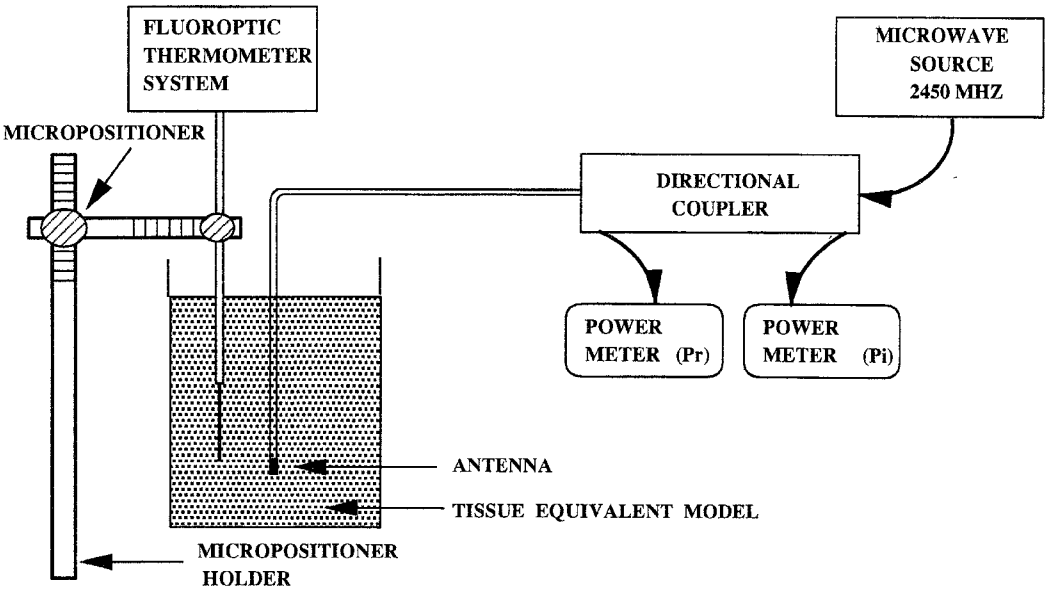

Fig 3 Schema of the experimental setup for measuring the temperature profile produced by a microwave antenna embedded in a tissue equivalent material. The temperature probe is moved inside the gel by using a micropositioner.

can be noted between our simulation results and the reported experimental and simulation results over a wide frequency range.

IV. Experimental Validation

To validate the computed temperature distributions, experiments were carried out by applying microwave power at 2450 MHz to a catheter prototype embedded in a cylindrical medium made of tissue equivalent material. A schema of the experimental setup is shown in Fig. 3. The gel phantom which modeled the cardiac tissue was placed in a polystyrene cylindrical container. The dielectric and thermal properties of the phantom material closely approximate those of cardiac tissue over the temperature range of interest [16]. The phantom material consisted of water (75.48%), NaCl (1.05%) for adjusting the electrical conductivity, polyethylene powder (15.01%) to reduce the dielectric constant of water, and a solidifying agent TX-151 (8.46%). The phantom had a height of 100 mm and a radius of 37 mm. Using a six-port reflectometer with an open-ended coaxial probe [17], the complex permittivity of the phantom material was measured over a frequency range of 915–2450 MHz at two different temperatures (30° and 60°C) and we found only a slight increase in the electrical conductivity. This phenomenon, which was reported in the literature earlier [18], validates the use of a constant, temperature independent electrical conductivity for the model.

A fluoroptic thermometry system (Model 755 Luxtron Corporation, Mountain View, CA) consisting of 1 to 4 single sensor fiber optic probes (0.8 mm diameter, MSA) was used to record the temperature within the phantom material. This system provides a ±0.1°C accuracy. These nonconductive probes were used in order to avoid the perturbation of the electric field around the antenna. One probe was moved within the gel to measure the temperature vertically along the symmetry axis, one was moved radially, and another remained fixed near the catheter tip. The probes were mounted on a submillimeter scaled 3-D micropositioner.

A. S11 Coefficient

The electrical accuracy of the numerical results was verified by using four prototypes of loaded monopoles with different active lengths in order to study the effect of this parameter on the reflected power. Each antenna was mounted on a coaxial cable (RG 316) with an outer diameter of 2.4 mm and a 50 Ω characteristic impedance. This kind of coaxial cable was chosen because its flexibility, size, and power handling capacity (about 100 W at 1–3 GHz) are acceptable for a microwave catheter. Each prototype was made by stripping the cable jacket and the outer conductor of the coaxial cable according to the following active lengths: 2, 6, 10, and 15 mm. A brass cap with a 3.5 mm length was then soldered to the inner conductor after completely covering the active region of the antenna with Teflon. Measurements of S11 were done with the antenna embedded in the phantom. The antennas penetrated at least 3 cm below the surface to eliminate the effect of the discontinuity at the air–gel interface. Fig. 4 shows the computed reflection coefficients as a function of the active length. The same graph illustrates the measured S11 using a network analyzer (HP 8510). Measurements were corrected for the cable losses (≈ 0.5 dB/ft). There is a good agreement between the numerical and experimental S11 values. At 915 MHz, the insulated loaded monopole is well matched for a 6–8 mm active length, whereas at 2450 MHz, the S11 exhibits a low value for an active length varying from 2 to 7 mm.

B. Temperature Measurements

Using a 10 mm loaded monopole terminated by a brass cap, the time course of the temperature and the steady-state axial and radial temperature profiles were measured within

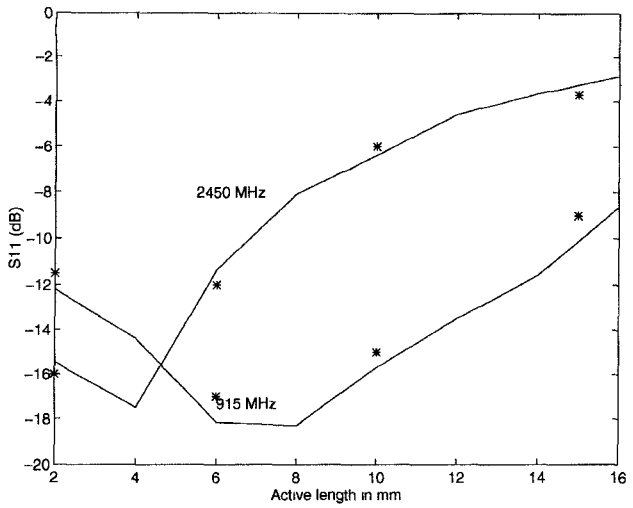

Fig. 4. Magnitude of the reflection coefficient S11 as a function of the active length of the monopole for two frequencies: 915 and 2450 MHz. The asterisks (*) represent the measured values, whereas the solid lines represent the simulation results.

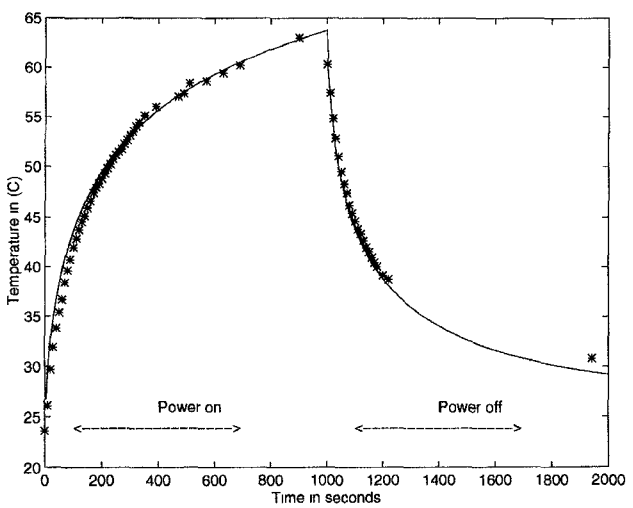

Fig. 5. Time course of the temperature recorded at 2 mm away from the antenna tip. Microwave power (4.2 W) was applied for 1000 s and then switched off. The asterisks (*) represent the recorded temperature, whereas the solid line represents the simulation result.

the phantom with the antenna embedded at the center of the container, 75 mm below the surface of the gel. Fig. 5 shows the time course of the temperature measured at 2 mm from the antenna tip with a probe glued to the coaxial cable, and the corresponding computed temperature. The microwave power was applied for a period of 1000 s and the temperature was recorded during 1000 more seconds. At $t = 0$, the initial gel temperature reflected the room temperature ($\approx$23°C) and after $t = 1000$ s, the gel was allowed to cool down for several minutes by thermal conduction and air convection. For this reason, air cooling was taken into account in the numerical computations by assuming a slow laminar air flow at room temperature around the cylinder. The curve shows a good agreement between the calculated and the measured temperatures which have an exponential shape during both the heating and the cooling processes.

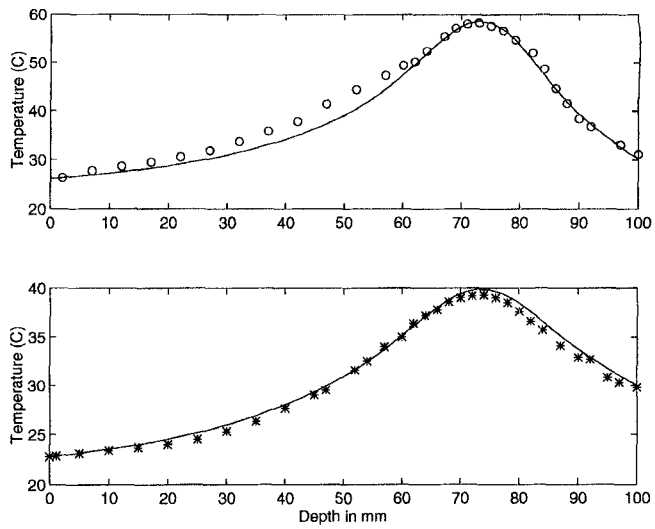

Fig. 6. Axial steady-state temperature profiles at two different radial distances. The upper graph represents the temperature profile at a radial distance $r = 5.25$ mm from the coaxial line surface, whereas the lower graph correspond to $r = 9.25$ mm. The upper surface of the phantom corresponds to 0 mm. The symbols (* and o) correspond to experimental values, whereas the solid lines represent the simulated temperature. The net power is 4.7 W for both profiles.

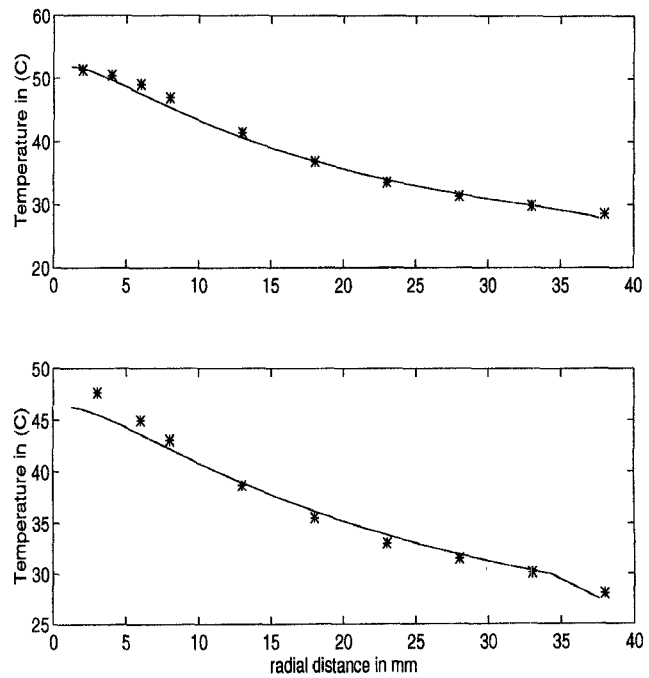

Fig. 7. Radial steady-state temperature profiles at two depths below the gel surface. The upper graph corresponds to $z = 5.5$ cm, and the lower corresponds to $z = 6.2$ cm. The asterisks (*) correspond to the experimental values, and the solid lines to the simulated temperature. The net power is 4.00 W for both profiles.

For the measurement of axial temperature profiles, the power was turned on for a few minutes until the temperature measured at the catheter tip reached a steady-state value. Fig. 6 shows two axial temperature profiles with the other temperature probe penetrating the phantom vertically along the symmetry axis and moving at 9.25 and 5.25 mm away from the coaxial cable surface, and the corresponding computed temperature profiles. The measurement sites were chosen close

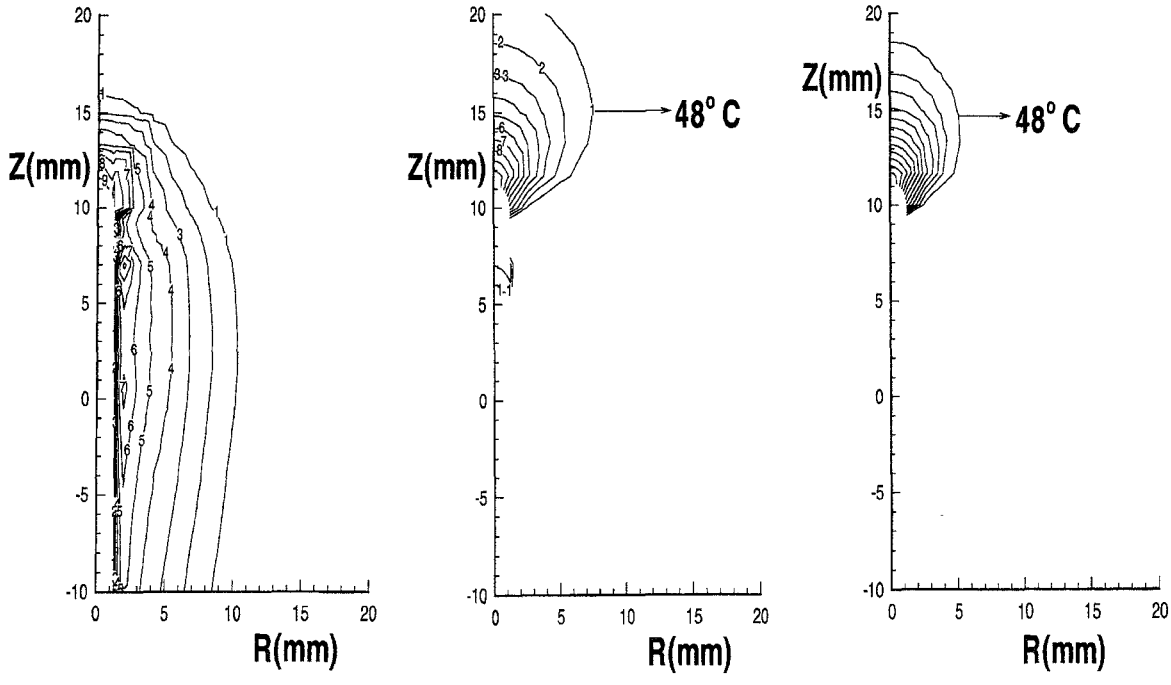

Fig. 8. (a) The SAR contour levels for an antenna with a 7 mm active length positioned in the heart model shown in Fig. 1. The outer conductor of the coaxial cable ends at $z = 0$ mm and the myocardium layer starts at $z = 10$ mm. (b) The isotherm contours lines in the myocardium for a frequency of 2450 MHz. The blood cavity is considered to be an isotherm pool at 37°C. The 48°C isotherm, which may correspond to an area of irreversible tissue damage, is indicated (c) The isotherm contour lines corresponding to a frequency of 915 MHz.

to each other where the temperature gradient exhibited a high value along the length of the radiating slot. The heating pattern dropped abruptly beyond the antenna tip and extended back along the antenna feedline producing a broad peak with a width proportional to the active length of the antenna.

Two radial temperature profiles measurements were also performed at two different depths from the gel surface to verify the radial extent of the heating pattern. Each measurement was repeated three times in order to average out the positioning error of the temperature probe. Fig. 7 shows the experimental and the calculated radial temperature profiles. The radial temperature fell off less sharply than the axial one as shown in the preceding figure. Again, the computed temperature profiles correspond well with the measured profiles.

V. Effect of Blood Masses

The complex permittivity of human blood is very similar to that of the myocardium [4], which implies that the electrical responses of the cardiac tissues and of the blood are almost the same. By using a homogeneous dissipative medium, we do not lose accuracy in the computation of the electromagnetic absorption process. However, the presence of blood flow complicates the interpretation of the SAR pattern. We can investigate the importance of this factor by computing the SAR contour lines for a loaded monopole with a 7 mm active length and a 3.5 mm cap length. With 30 W of net power applied, the SAR contour lines shown in Fig. 8(a) exhibit two peaks: one at the antenna tip and one at the junction with the coaxial cable. The SAR decreases quite abruptly in the upper part close to the catheter tip while presenting a slower decay in the radial direction. At least 70% of the power is dissipated in the blood cavity for this particular catheter configuration (perpendicular to the myocardium). To study the relation between the SAR distribution and the lesion shape, the isotherms were computed by taking into account the heat exchange process between the myocardium and blood flowing with a steady laminar flow at 37°C. The isotherms are shown in Fig. 8(b), the maximum myocardial temperature is 85°C and the 48°C isotherm gives an indication of the extent of irreversible tissue damage [19]. Blood flow produces a significant effect on the temperature distribution within the myocardium by acting as a heat sink capable of drawing significant thermal energy away from the ablation target. This results in a meniscus-shaped lesion. To compare the effects of using a frequency of 915 MHz instead of 2450 MHz, power (25 W) was applied to the same catheter model to reach the same maximum myocardial temperature (85°C). The estimated lesion at 915 MHz, shown in Fig. 8(c), exhibits the same shape as the previous one except that its extent is smaller. These results suggest that 2450 MHz is a frequency that can produce a larger lesion even though the reflection coefficient is lower than at 915 MHz (cf. Fig. 4). Knowing that the penetration depth of an electromagnetic wave is higher at 915 MHz than at 2450 MHz, these results are not general and depend on this particular antenna and orientation because the radiation pattern is more broadsided at 915 MHz than at 2450 MHz.

VI. Discussion and Conclusion

An insulated monopole terminated by a metallic cap was modeled and tested experimentally in a tissue phantom in

order to validate an electrothermal model for the simulation of microwave cardiac ablation. The use of this type of material has different advantages such as the reproducibility of the experiment results, the facility to record the temperature inside the material with a moving probe, and the possibility for repeated applications of microwave power because the tissue equivalent material maintains its thermal and dielectric properties after several applications.

In our models, we have neglected the convective heat loss due to the microvascular blood flow. In cancer thermotherapy [20], broad regions are heated to 42–44°C and the microvessels exhibit a hyperemic response that accounts for an increased convective heat loss. In contrast, during cardiac catheter ablation where the maximum temperature can reach 100°C, blood coagulates and the microvessels are disrupted within the zone of tissue injury and just outside the lesion border [21]. Therefore, the contribution of microvascular blood flow to the thermodynamics of lesion formation is likely to be negligible [22]. This assumption is experimentally supported by the observations of Haines and Watson [19] who found no significant difference in steady-state temperature distribution during normal coronary artery flow and during temporary interruption of coronary flow during RF energy application in isolated perfused canine myocardium.

Our simulation results on the effects of the length of the radiating section on the reflection coefficient agree very well with our experimental results and with the results reported in another study [10]. Our model can thus be used to determine optimum antenna dimensions which minimize the reflected power due to the impedance mismatch between the feedline and the antenna. Other antenna designs, such as antennas with multiple slots, for example, could also be investigated as long as the antenna remains axisymmetrical. This could lead to matched antennas producing lesions with different geometries that are well suited to the specific arrhythmogenic substrate, such as elongated lesions for atrial flutter or small hemispherical lesions for accessory pathways in patients with the Wolff–Parkinson–White syndrome [1]. The antenna used in the present study is one of many possible designs: the slot length was adjusted to minimize reflected power (Fig. 4), whereas a cap length of 3.5 mm was selected because it is the usual length for RF catheters and it could be increased to dissipate more power near the tip of the catheter. This particular antenna was selected for validation purposes and it constitutes a compromise between broadside-fire and end-fire radiation patterns: in our simulations, the power dissipated within the myocardium is not high (30%) because the catheter is perpendicular to the ventricular surface but in clinical applications, the catheter would form a smaller angle with a concave endocardial surface, and the power dissipated within the myocardium would be larger.

In all experiments, the measured temperature was in good agreement with the computed temperature profile—typically within a few percent. For the axial temperature profile, the temperature showed a high gradient in the vicinity of the radiating section and decreased rapidly beyond the antenna tip, while it decreased more slowly radially. The estimation of the geometry of the lesion from these temperature distributions can be approximated to some extent by considering a critical temperature of 48°C above which irreversible tissue damage was experimentally observed by Haines and Watson [19]. According to the tissue damage function proposed by Henriques [23], the required exposure time to damage a tissue at 47°C is more than 1 h, whereas it is a few minutes at 49°C, which corresponds to the time required to reach a steady state for cardiac catheter ablation. Also, Whayne *et al.* [4] have shown in their experimental comparison between radiofrequency and microwave cardiac ablation that a hyperthermic exposure duration of up 10 min did not result in a significant increase in myocyte death with respect to a 4–5 min exposure. The relationship between tissue damage and tissue temperature constitutes a complex, nonlinear, and time-dependent process. The role of modeling thus appears, for the moment, better suited to the comparison between the heating patterns of different antennas than to the accurate prediction of the extent of the lesions.

Microwave catheter ablation constitutes a new surgical modality with a potential to produce larger lesions than RF energy [4], [9]. Microwave catheter ablation may also be exempted of some of the complications associated with energy delivery by RF conduction currents, such as the formation of a coagulum over the catheter tip at high temperatures which increases the electrode impedance and severely impairs energy delivery. The proposed model, with its experimental validation, can lead to a better understanding of RF and microwave energy delivery in the heart as well as to the development of new catheters with optimized antenna designs.

ACKNOWLEDGMENT

The authors wish to thank M. D. Bérubé for the measurements of the complex permittivity of the phantom material, and M. C. Akyel for the temperature instrumentation.

REFERENCES

[1] W. M. Jackman, X. Wang, and K. J. Friday, "Catheter ablation of accessory atrioventricular pathways (Wolff–Parkinson–White syndrome) by radiofrequency current," *N. E. J. Med.*, vol. 324, pp. 1605–1611, 1991.

[2] M. Scheinman, "North American Society of Pacing and Electrophysiology (NASPE) survey on radiofrequency catheter ablation: Implications for clinicians, third party insurers, and government regulatory agencies," *PACE*, vol. 15, pp. 2228–2231, 1992.

[3] W. Kaltenbrunner, R. Cardinal, M. Shenasa, M. Dubuc, R. A. Nadeau, G. Tremblay, P. Savard, and P. Pagé, "Computerized mapping of epicardial and endocardial activation during sustained monomorphic ventricular tachycardia in patients with myocardial infarction: the epicardial/endocardial relationship," *Circ. Res.*, vol. 84, pp. 1058–1071, 1991.

[4] J. G. Whayne, S. Nathan, and D. E. Haines, "Microwave catheter ablation of myocardium *in vitro*," *Circulation*, vol. 89, pp. 2390–2395, 1994.

[5] R. M. Rosenbaum, A. J. Greenspon, S. Hsu, P Walinsky, and A. Rosen, "RF and microwave ablation for the treatment of ventricular tachycardia," in *IEEE MTT-S Dig.*, Atlanta, 1993.

[6] J. W. Strobhen, E. D. Bowers, E. J. Walsh, and E. B. Douple, "An invasive microwave antenna for locally-induced hyperthermia for cancer therapy," *J. Microwave Power*, vol. 14, pp. 339–350, 1979.

[7] M. F. Iskander and A. M. Tumeh, "Design optimization of interstitial antennas," *IEEE Trans. Biomed. Eng.*, vol. 36, pp. 238–246, Feb. 1989.

[8] G B. Gentili, M. Leoncini, B. S. Trembly, and S. Schweizer, "FDTD electromagnetic and thermal analysis of interstitial hyperthermic applicators," *IEEE Trans. Biomed Eng.*, vol. 42, pp. 973–980, 1995.

[9] A. Khebir, Z. Kaouk, and P. Savard, "Modeling a microwave catheter antenna for cardiac ablation," in *IEEE MTT-S Dig.*, Orlando, 1995.
[10] S. Labonté, H. O. Ali, and L Roy, "Monopoles for microwave catheter ablation of heart tissue," in *IEEE MTT-S Dig.*, Orlando, 1995, pp. 303–306.
[11] P P. Silvester and R. L Ferrari, *Finite Elements for Electrical Engineers*. Cambridge: Cambridge University Press, 1983
[12] J. F. Lee, G. M. Wilkins, and R. Mittra, "Finite-element analysis of axisymmetric cavity resonator using a hybrid edge element technique," *IEEE Trans. Microwave Theory Tech.*, vol. 41, pp. 1981–1987, 1993.
[13] J. S. Wang and R. Mittra, "Finite element analysis of MMIC structures and electronic packages using absorbing boundary conditions," *IEEE Trans. Microwave Theory Tech.*, vol. 42, pp. 441–449, 1994.
[14] Z. Kaouk, A. Shahidi, P. Savard, and F Molin, "Modelling of myocardial temperature distribution during radiofrequency ablation," *Med. Biol. Eng Comput.*, vol. 34, pp. 1–6, 1996.
[15] S. Labonté, "A computer simulation of radio-frequency ablation of the endocardium," *IEEE Trans. Biomed. Eng.*, vol. 41, pp. 883–889, Sept. 1994.
[16] C. K. Chou, G. W. Chen, A. W. Guy, and K. H. Luk, "Formulas for preparing phantom muscle tissue at various radiofrequencies," *Bioelectromagnetics*, vol. 5, pp 435–441, 1984.
[17] F. M. Ghannouchi and R. G. Bosisio, "Measurement of microwave permittivity using a six-port reflectometer with an open-ended coaxial line," *IEEE Trans. Instr. Meas.*, vol 38, pp. 505–508, 1989.
[18] K. R. Foster and J. L. Schepps, "Dielectric properties of tumor and normal tissues at radio through microwave frequencies," *J. Microwave Power*, vol. 16, pp. 107–119, 1981.
[19] D. E. Haines and D. D. Watson, "Tissue heating during RF catheter ablation: A thermodynamic model and observations in isolated and superfused canine right ventricular free wall," *PACE*, vol. 12, pp. 962–976, 1989.
[20] T. E. Dudar and R. K. Jain, "Differential response of normal and tumor microcirculation to hyperthermia," *Cancer Res.*, vol. 44, pp. 605–612, 1984.
[21] S. Nath, W. Glasheen, J. G. Whayne, *et al*, "Radiofrequency catheter ablation results in a reduction in myocardial microvascular blood flow: Insights into the patho-physiology of lesion extension over time" (abstract), *J. Amer. Coll. Cardiol.*, vol. 19, no. 26A, 1992.
[22] D. E. Haines, "The biophysics of radiofrequency catheter ablation in the heart," *PACE*, vol. 16, pp. 586–591, 1993.
[23] F C Henriques, "Studies of thermal injury," *Archives Pathol.*, vol. 5, pp. 489–502, 1947.

Zouheir Kaouk, photograph and biography not available at the time of publication.

Ahmed Khebir, photograph and biography not available at the time of publication.

Pierre Savard, photograph and biography not available at the time of publication.